

Numerical Simulation of the Effect of Trees on Downwind Noise Barrier Performance

T. Van Renterghem, D. Botteldooren

Department of Information Technology, Ghent University, St. Pietersnieuwstraat 41, 9000 Gent, Belgium

Summary

Simulating sound propagation outdoors in time-domain taking into account the effect of wind by means of steady-state Computational Fluid Dynamics (CFD) has recently shown to be very useful. In this paper, the important effect of wind on noise barrier performance and the effect of rows of trees to improve wind profiles around noise barriers are modelled. A finite-difference time-domain simulation model is adapted for sound propagation outdoors in a complex, non-uniform background flow. The simulation of a typical traffic noise situation, where at either side of a line source a noise barrier is present, needs appropriate, non-reflecting boundary conditions like Perfectly Matched Layers (PML) to limit the simulation domain. The PML method is extended for sound propagation in background flow. The numerical model is validated based on two wind tunnel experiments at scale. These show that the model can be used successfully to simulate both the screen-induced refraction of sound and the effect of windscreens to improve downwind noise barrier performance. The influence of parameters involved like the porosity of the canopy of the trees, wind speed and distance between source and noise barrier were studied. Global effects of different configurations of windscreen for typical traffic noise are evaluated in an area of interest behind the downwind noise barrier, exceeding the study region in the wind tunnel experiments.

PACS no. 43.50.Gf, 43.28.Js, 43.28.Fp, 43.28.Gq

1. Introduction

The efficiency of noise barriers in downwind direction decreases strongly due to wind. The wind flow will impose a large pressure drop over the noise barrier. As a result, high wind speeds are observed above the barrier, while the atmosphere is at rest just behind the barrier. As a consequence, there will be large, positive gradients in the wind speed resulting in a refraction of sound in downward direction. This phenomenon is called the screen-induced refraction of sound, and has been analysed by many authors both in calculations and in experiments, e.g. [1, 2, 3, 4].

To cope with this problem, Heimann and Blumrich [5] performed calculations of various screen geometries in wind. Global effects were rather small and it is expected that the construction of such (complicated) screens would be rather expensive compared to thin rectangular noise barriers. This solution can not be applied to the many kilometres of noise barriers already present along roads. The use of trees to reduce wind speed behind a noise barrier was proposed by Van Renterghem and Botteldooren. In both a wind tunnel experiment at scale [6] and in a field experiment along a highway [7], the improvement of noise barrier performance by changing local wind profiles using trees was demonstrated for downwind sound propaga-

tion. Both experiments indicate that placing trees behind noise barriers could be a good, practical solution. Important advantages are the possibility to treat existing noise barrier configurations and the fact that this is a relatively inexpensive measure. To numerically simulate the effect of windscreens on noise barrier performance, an accurate description of the complex flow field in the vicinity of the combination of noise barrier(s) and windscreens must be included. The sound propagation model has to take into account this detailed flow information.

Sound propagation in an inhomogeneous outdoor atmosphere has been investigated intensively. Most models do not intend to be complete aero-acoustic models. The aim is to predict the influence of gradients in sound speed on sound propagation caused by gradients in both wind speed and temperature. Also topography and turbulent effects are important issues. Since propagation distances are in general large (up to some kilometres), one has to find efficient calculation methods, without neglecting important meteorological influences.

Sound propagation in a layered atmosphere is usually computed in frequency-domain. An overview of the most frequently used models for outdoor sound propagation can be found e.g. in references [8] and [9]. A simulation technique that can handle variations both in sound speed profiles and ground impedance along the propagation path is the Parabolic Equation (PE) method. This method however takes in account only the wind velocity in the direction of propagation i.e. the effective speed of sound. Near

Received 19 November 2002,
accepted 19 May 2003.

barriers however, also vertical flow is present and this effect is disregarded. Another important drawback of the PE is that one-way sound propagation is described: only the sound waves travelling in the direction from the source to the receiver are allowed for. When a source is situated in between two partially reflecting noise barriers as often encountered in traffic noise situations, the multiple reflections and their interactions can not be modelled. Recently the boundary element (BE) method is extended for the use in a layered atmosphere based on the normal modes solution in a downward refracting atmosphere [10]. The normal mode solution assumes a specific sound speed profile, for which an analytical solution can be obtained. When receiver heights are small in comparison to the ray of curvature, this sound speed profile approximates a linear one [11]. This BE approach however can not model variations in the sound speed profiles along the propagation path.

In this paper we adapt the Finite-Difference Time-Domain (FDTD) simulation technique (e.g. [12, 13]) for sound propagation in background flow, obtained by Computational Fluid Dynamics (CFD). This method is similar to the linearized Euler (LE) model described by Blumrich and Heimann [14]. Sound propagation is described in a time-invariant background flow. This approach for the calculation of sound propagation in an inhomogeneous atmosphere has shown to be of practical use for different applications outdoors [14]. Because the model used here was developed independently and with focus on the screen-induced refraction of sound over barriers in presence of trees, some approximations are different. Details on both the mathematical model and discretisation are therefore given in this paper. The FDTD model presented in this paper can easily be used for irregular ground surfaces. When the magnitude of elevations and depressions are small in comparison with the spatial discretisation, grid refinements may be applied. Changing ground characteristics with distance can easily be included. Effects of topography will not be investigated explicitly in this paper.

The effect of temperature gradients can be taken into account in the FDTD model. In this paper however, the focus is on the effect of wind on noise barrier performance. The influence of the temperature profiles is not considered here.

The paper is outlined as follows. In first place, the mathematical derivation of the equations for sound propagation in a background flow is presented. Some special adaptations have been made for outdoor sound propagation. The non-locally reacting ground model by Zwicker and Kosten [15] can be formulated in time-domain and has shown to be accurate based on a comparison with frequency-domain techniques for sound propagation over finite impedance ground [16]. The important issue of perfectly absorbing boundary (PAB) conditions to border a simulation domain is addressed. The accuracy of our model to simulate sound propagation over a perfectly hard, screened ground for a normal incident wind direction and various wind speeds will be proven. A wind tunnel experiment performed by Salomons [3] will be used for that pur-

pose. The numerical scheme presented here will be compared to the PE calculations of Salomons [3], as well as to simulation with the linearized Euler model by Blumrich and Heimann [14].

The main purpose of this paper is to simulate numerically the influence of the presence of windscreens or rows of trees on noise barrier performance in wind. The simulations will first be compared to the experimental results obtained in a wind tunnel experiment [6]. Finally, the effect of the most important parameters will be analysed, for different frequency bands and typical traffic noise spectra, using the numerical model.

2. Mathematical model for sound propagation in background flow

The basic fluid equations, the conservation of momentum (equation 1) and the conservation of mass (equation 2) are used as a starting point to derive the equations for sound propagation in background flow:

$$\rho_t \left[\frac{\partial \mathbf{v}_t}{\partial t} + (\mathbf{v}_t \cdot \nabla) \mathbf{v}_t \right] + \nabla p_t = 0, \quad (1)$$

$$\frac{\partial \rho_t}{\partial t} + \nabla \cdot (\rho_t \mathbf{v}_t) = 0, \quad (2)$$

where p_t is the fluid pressure, \mathbf{v}_t is the fluid velocity vector, and ρ_t is the fluid density.

2.1. Velocity equation

From numerical fluid mechanics, it is known that the discretised form of equation (1) does not ensure kinetic energy conservation [17]. A different form of the momentum equation will therefore be derived, where the kinetic energy term is explicit. This alternate form of conservation equation (1) also makes the rotor of the velocity explicit, which will be used further in this section. This alternate form is obtained by applying the vector identity $\nabla(\mathbf{a} \cdot \mathbf{a}) = 2[\mathbf{a} \times (\nabla \times \mathbf{a}) + (\mathbf{a} \cdot \nabla)\mathbf{a}]$ to equation (1):

$$\rho_t \left[\frac{\partial \mathbf{v}_t}{\partial t} - \mathbf{v}_t \times (\nabla \times \mathbf{v}_t) \right] + \nabla p_t + 0.5 \rho_t \nabla(\mathbf{v}_t \cdot \mathbf{v}_t) = 0. \quad (3)$$

Pressure, fluid density and fluid velocity are split into two contributions:

$$\rho_t = \rho_0 + \rho, \quad (4)$$

$$\mathbf{v}_t = \mathbf{v}_0 + \mathbf{v}, \quad (5)$$

$$p_t = p_0 + p, \quad (6)$$

where ρ_0 is the ambient density, ρ is the acoustic part of the density, \mathbf{v}_0 is the background fluid velocity, \mathbf{v} is the acoustic part of the fluid velocity, p_0 is the ambient pressure, and p is the acoustic pressure.

Some simplifications are made concerning the background flow. It is assumed that the fluid flow is quasi-static ($\partial \mathbf{v}_t / \partial t = 0$ and $\partial \rho_0 / \partial t = 0$) and incompressible

($\nabla \rho_0 = 0$). This is allowed because the acoustic perturbations, for which compressibility is essential, are considered separately. Isothermal flow is supposed: the speed of sound c is independent of place and time.

Following assumptions regarding the acoustic part of the equations are made. In this paper only linear acoustics are considered. Source terms i.e. all terms that do not contain the acoustic quantities are neglected. The linearised velocity equation without source terms reads

$$\rho_0 \left[\frac{\partial \mathbf{v}}{\partial t} - \mathbf{v} \times (\nabla \times \mathbf{v}_0) - \mathbf{v}_0 (\nabla \times \mathbf{v}) \right] + \rho [(\mathbf{v}_0 \cdot \nabla) \mathbf{v}_0] + \nabla p + \rho_0 \nabla [\mathbf{v} \cdot \mathbf{v}_0] = 0. \quad (7)$$

Until now the fact that \mathbf{v} and p are the acoustic part of the flow field is not explicitly used. Like any vector field the acoustic velocity field \mathbf{v} can be written as:

$$\mathbf{v} = \nabla \phi + \nabla \times \mathbf{A} = \mathbf{v}_g + \mathbf{v}_r, \quad (8)$$

where ϕ is the well-known velocity potential, and $\nabla \times \mathbf{A} = \mathbf{v}_r$ is the rotational part of the field. In an isotropic medium at rest with an acoustic perturbation, \mathbf{v}_r equals zero. Also remark that \mathbf{v}_r does not influence the acoustic pressure equation directly. The initial assumption (5) that \mathbf{v} is the acoustic part of the velocity now translates to $\mathbf{v}_g \gg \mathbf{v}_r$. Using equation (8), the magnitude of the first terms of equation (7) can be compared. This results in

$$\mathbf{v}_0 \times (\nabla \times \mathbf{v}) \ll \frac{\partial \mathbf{v}}{\partial t}, \quad (9)$$

when Mach numbers are skaller than 1 and the time dependence of \mathbf{v}_g corresponds to acoustic frequencies. It is important to explicitly introduce this condition on \mathbf{v} since failure to do so allows the acoustic part of the velocity to evolve to containing parts of the fluid flow, thus introducing unwanted complexity in the numerical simulation. Not making equation (9) explicit results in unstable simulations for large flow velocities and complex flows, as was observed during numerical experiments.

Since the background flow is assumed to be time-invariant and incompressible, it follows from the conservation of momentum equation, applied to the background flow, that the fourth term in equation (7) must equal zero.

Using the above made assumptions, the velocity equation reads

$$\frac{\partial \mathbf{v}}{\partial t} - \mathbf{v} \times (\nabla \times \mathbf{v}_0) + \frac{1}{\rho_0} \nabla p + \nabla [\mathbf{v} \cdot \mathbf{v}_0] = 0. \quad (10)$$

In this equation, coupling between acoustics and flow is limited. Fluid flow results in convection and refraction of acoustic waves. Generation of sound by the flow on the other hand is not considered, since source terms in the previous equations (Lighthill-equivalents) are neglected. It is further assumed that acoustic fields do not influence the background flow. Therefore, background fluid velocity can be calculated using standard CFD (Computational Fluid Dynamics) software [18], and is assumed to be known during the acoustic calculations.

2.2. Pressure equation

In the conservation of mass equation (2), the flow quantities are also split in an acoustic part and a part attributed to the background flow. Linearisation in acoustic quantities, assuming a time-invariant background flow and neglecting source terms results in

$$\frac{\partial \rho}{\partial t} + \nabla \cdot \rho \mathbf{v}_0 + \nabla \cdot \rho_0 \mathbf{v} = 0. \quad (11)$$

The divergence of the background flow must equal zero due to the assumption of incompressibility and time independence of the background flow ($\nabla \cdot \mathbf{v}_0 = 0$). This is a direct consequence of the conservation of mass equation applied to the background flow. Disobeying this condition would lead to large errors. Indeed: suppose a static fluid flow in combination with non-zero divergence in the background flow. Because the fluid cannot be compressed and the flow pattern is time-independent, on certain places the pressure would go to infinity. Of course, this assumption may be enforced during the calculation of the background velocity field. But due to numerical inaccuracy and interpolations (e.g. when the acoustic grid and background velocity grid do not fit), this is not always guaranteed for the numeric flow field actually inserted in the acoustic equations. For these reasons, this condition is made explicit.

The linear pressure-density relation $p = c^2 \rho$ is used, where c represents the adiabatic sound speed. Using the above-mentioned assumptions, an equation is obtained for the calculation of the acoustic pressure in time-domain:

$$\frac{\partial p}{\partial t} + c^2 \rho_0 \nabla \cdot \mathbf{v} + \mathbf{v}_0 \nabla p = 0. \quad (12)$$

3. Finite-difference time-domain model

The use of a staggered grid has shown to have particular advantages for acoustic simulations [12]. In a Cartesian grid, the acoustic pressures are determined in the centres of the FDTD cells, at the grid positions ($i \, dx, j \, dy, k \, dz$) at sampled times $l \, dt$. The three components of the particle velocity are calculated at the surfaces that border each cell, respectively at staggered grid positions ($(i + 0.5) \, dx, j \, dy, k \, dz$), ($i \, dx, (j + 0.5) \, dy, k \, dz$) and ($i \, dx, j \, dy, (k + 0.5) \, dz$), at intermediate times $(l + 0.5) \, dt$. To indicate spatial discretisation steps, dx , dy , and dz are used, while dt is the time discretisation step. The indices i , j , and k locate the spatial points, the index l is used for discrete time.

In the absence of background flow, central difference approximations are well suited to discretise the equations in this staggered grid. In a first order scheme, the velocity at time $(l + 0.5) \, dt$ only depends upon the velocity at the previous time $(l - 0.5) \, dt$ and the discretised pressure at the time $l \, dt$ in adjacent positions. Amongst other advantages, this allows for in place computation (the new value replaces the old one in computer memory) and thus an important reduction of memory storage. To keep the simulations stable, the Courant number needs to be smaller

than one [12]. The method can be easily extended to more general grids [12]. When a background flow is present, time and space matching of the staggered grid no longer emerges naturally. To ensure stability and accuracy, more care is needed concerning the discretisation of the equations.

Discretising the acoustic pressure equation (12) in time yields

$$p^{l+1} + 0.5dt(\mathbf{v}_0 \cdot \nabla p^{l+1}) = p^l - dt c^2 \rho_0 (\nabla \cdot \mathbf{v}^{l+0.5}) - 0.5dt(\mathbf{v}_0 \cdot \nabla p^l). \quad (13)$$

The unknown pressure field at time $(l + 1) dt$ is calculated based on the values of the previous pressure field $l dt$ and on the acoustic velocity field of the intermediate time step $(l + 0.5) dt$. However, when discretising the spatial derivatives of the left-hand side, neighbouring values of p will be involved. This would ultimately lead to a band matrix to be inverted at each time step. Since numerical efficiency is of primary concern in this work, an alternative approximation is chosen. The spatial derivatives at the left-hand side of equation (13) are numerically calculated based on an approximation of the sound pressure that neglects the background flow:

$$p_{\text{appr.}}^{l+1} \approx p^l - dt c^2 \rho_0 (\nabla \cdot \mathbf{v}^{l+0.5}). \quad (14)$$

This approximation corresponds to neglecting second order terms in the Mach number ($M = v_0/c$), and is sufficiently accurate for flow velocities encountered outdoors. Just before time $(l + 1) dt$, equation (14) is used for the calculation of the second term on the left-hand side of equation (13). The discretisation of the velocity equation is based on the same approach, and will therefore not be discussed here.

4. Adaptations for outdoor sound propagation

4.1. Ground models

A perfectly hard material is easily modelled in an FDTD grid. On such a boundary, the orthogonal component of the acoustic velocity is zero. A locally reacting physical boundary can be described by a surface impedance $Z(\omega)$. In reference [19] it is shown that a complex impedance of the form

$$Z(\omega) = Z_0 + Z_1 j\omega + \frac{Z_{-1}}{j\omega}, \quad (15)$$

where j equals $\sqrt{-1}$, can be fitted in the FDTD calculation scheme and is a good approximation to most frequency dependent impedances over at least a few octave bands. The second term in equation (15) corresponds to a time-derivative, while the third term can be approximated by integration in time. Both can easily be discretised. Such a boundary condition is numerical efficient, since the calculation grid does not have to be extended.

Several models can be used for the description of sound propagation inside the ground, e.g. the models proposed by Biot [20] and Zwikker and Kosten [15]. The latter proposed linear equations for sound propagation in porous media, to which many outdoor grounds can be categorised. In this model, only the air in between the soil particles is the propagation medium. The soil particles form a rigid frame. The ground surface in such a model is called non-locally reacting or extended-reacting. It was shown in reference [16] that the model by Zwikker and Kosten can be used for accurately modelling sound propagation over finite impedance grounds. Besides, the model described in reference [15] is easy to implement in the finite-difference time-domain scheme. This model uses three ground parameters: flow resistivity R , porosity φ and the structure factor k_s . The time-domain equations for acoustic velocity and pressure in time-domain in soil are [15]:

$$\nabla \cdot p + \rho' \frac{\partial v}{\partial t} + Rv = 0, \quad (16)$$

$$\frac{\partial p}{\partial t} + p' c'^2 \nabla \cdot v = 0, \quad (17)$$

where $\rho' = \rho_0 k_s / \varphi, \quad (18)$

$$c' = c_0 / \sqrt{k_s}. \quad (19)$$

In these equations, a damping term is used based on the flow resistivity. The mass density of the soil ρ' and the speed of sound in the ground c' are adapted using the porosity and structure factor of the ground.

In the finite-difference time-domain implementation, no conditions concerning homogeneity of the soil were imposed. Effects like compacting of soils can be easily modelled by increasing e.g. porosity with depth within the ground.

4.2. Perfectly absorbing boundary conditions

In outdoor sound propagation simulations, the calculation domain is usually not physically bounded. The unlimited propagation region has to be truncated to limit the simulation domain. This truncation may not influence the acoustic calculations: reflections are not allowed. So-called ‘‘perfectly absorbing boundary’’ (PAB) conditions must be applied at the border of the simulation grid. For some special cases, the need for PAB’s can be circumvented by working with a broadband pulse [16]. By analysing the time-domain signal, the reflections from the non-physical boundaries can be removed. An important condition is that the non-physical boundaries and points of interest are sufficiently apart from each other so there is no overlap between signal of interest and unwanted reflections. Sound propagation over flat ground without screens and the use of a single noise barrier are examples for which this method can be used.

However, the specific case of a sound source in between two noise barriers, as often encountered in traffic noise situations, needs the application of PAB’s. Multiple reflections between the barriers will otherwise interfere with reflections from boundaries, resulting in inaccurate calcu-

lations. Very good PAB's namely the "Perfectly Matched Layers" (PML) were developed by Berenger [21] for electromagnetic FDTD simulations. However, these boundary conditions have not been extended to the case of sound propagation in background flow up to now.

When applying a PML (or Berenger boundary condition), the simulation domain has to be extended with a limited number of cells, in which a non-physical propagation occurs. Artificial damping coefficients κ are added to the acoustic equations for calculating the propagation in the Berenger layer. The derivation of the PML equations here assumes a uniform background flow, normal (= direction α) to the interface between the PML layer and propagating medium:

$$\frac{\partial p_{\perp}}{\partial t} + c^2 \rho_0 \frac{\partial v_{\alpha}}{\partial \alpha} + v_{0\alpha} \frac{\partial p_{\perp}}{\partial \alpha} + \kappa_{1,\perp} p_{\perp} = 0, \quad (20)$$

$$\frac{\partial p_{\parallel}}{\partial t} + c^2 \rho_0 \sum_{\gamma \neq \alpha} \frac{\partial v_{\gamma}}{\partial \gamma} + v_{0\alpha} \frac{\partial p_{\parallel}}{\partial \alpha} + \kappa_{1,\parallel} p_{\parallel} = 0, \quad (21)$$

$$p_{\perp} + p_{\parallel} = p, \quad (22)$$

$$\rho_0 \left[\frac{\partial v_{\alpha}}{\partial t} + v_{0\alpha} \frac{\partial v_{\alpha}}{\partial \alpha} \right] + \frac{\partial p}{\partial \alpha} + \kappa_{2,\perp} v_{\alpha} = 0, \quad (23)$$

$$\rho_0 \left[\frac{\partial v_{\beta}}{\partial t} + v_{0\alpha} \frac{\partial v_{\beta}}{\partial \alpha} \right] + \frac{\partial p}{\partial \beta} + \kappa_{2,\parallel} v_{\beta} = 0, \quad (24)$$

where β represents the coordinate directions, except for the direction of the uniform background flow, where γ runs over the 3 coordinate directions, unless exceptions are stated, where v is the acoustic velocity and $v_{0\alpha}$ is the uniform background flow velocity along coordinate axis α .

Splitting the acoustic pressure in an artificial component normal to the Berenger-interface (p_{\perp}), and a component parallel to the interface (p_{\parallel}) results in an additional degree of freedom. This split-field approach makes it possible to fully transmit plane waves at all angles of incidence to the Berenger layer. Note that p_{\parallel} and p_{\perp} are not physical quantities.

If the following conditions are satisfied, both media are perfectly matched:

$$\kappa_{2,\parallel} = \kappa_{1,\parallel} = 0, \quad (25)$$

$$\kappa_{1,\perp} = \kappa_{2,\perp} / \rho_0. \quad (26)$$

Some reflection will however occur in the discrete FDTD grid because of the abrupt change in damping. To reduce this discontinuity at the interface, Berenger [22] proposed to gradually change the material parameters along the normal axis on the interface, according to

$$\kappa_{1,\perp}(x) = \kappa_{1,\perp,\max} \left(\frac{x}{d_{PML}} \right)^m, \quad (27)$$

where x is the depth inside the layer normal to the interface and d_{PML} is the total thickness of the PML. It is found that the parameter m is preferably chosen between 3 and 4 [22].

The Berenger boundary condition is derived here for sound propagation in a uniform background flow. Assuming a logarithmic wind speed profile, important vertical

gradients are only present close to the ground surface. The use of the uniform flow PML equations in such a non-uniform flow will still be an important improvement relative to e.g. first order approximation PAB's.

To verify the accuracy, a normal incident plane wave on an optimised PML (with a thickness of 40 grid cells) is simulated. The spatial discretisation step in the grid was $1/10^{\text{th}}$ of the wavelength of the maximum frequency considered. The sound energy reflected was more than 120 dB lower than the incident energy.

5. Validation

5.1. Effect of wind on noise barrier performance

In a wind tunnel experiment at scale by Salomons [3], downwind sound propagation was studied for a normal incident wind direction. The ground surface was perfectly reflecting. At full scale, the screen height was 5.55 m, the source was positioned at a height of 1.89 m, 30 m before the screen. At one distance behind the noise barrier (60 m) and at two heights above the ground surface (6 m and 12 m), measurements were done. A sketch of the experimental set-up can be found in Figure 1. Wind speeds ranged from 2 m/s to 14 m/s, measured at a height of 9 m. At the entrance of the test section, the wind speed profile is logarithmic [3]:

$$v(z) = \frac{v_{z_{\text{ref}}}}{\ln(1 + z_{\text{ref}}/z_0)} \ln(1 + z/z_0), \quad (28)$$

where z is the height above the surface, v_z is the velocity at height z and z_0 is the roughness length. More details on this experiment can be found in the above-mentioned paper. Measurements of the effect of wind on the 250-Hz and 500-Hz octave band sound pressure levels are compared to simulations. In Figure 1, our results (FDTD) are compared to the experimental data, to the PE calculations performed by Salomons, and to the Linearised Euler (LE) model used by Blumrich and Heimann [14]. The effect of wind on noise barrier performance is shown with increasing (incident) wind speed, measured at a height of 9 m.

In general, the FDTD simulations agree well with the LE model. Because the FDTD and LE are very similar models, the differences in performance are surprising at first sight and their origin is therefore investigated. These differences probably arise from the calculation of flow profiles. When the same background flow field is used (shown by the * in Figure 1, for a wind speed of 10 m/s), the FDTD and LE model agree better, except for 500 Hz at 6 m. For the calculation of the flow field in our model, the (commercial) CFD software STAR-CD is used. A wide range of turbulence models could be used to minimise differences with measured wind speeds along the wind tunnel.

For the (low) frequency band of 250 Hz at a height of 6 m, the FDTD model results in some better agreement with measurements in comparison to the other models. At the receiver height of 12 m, both the FDTD and LE model approximate the experimental data better than the PE cal-

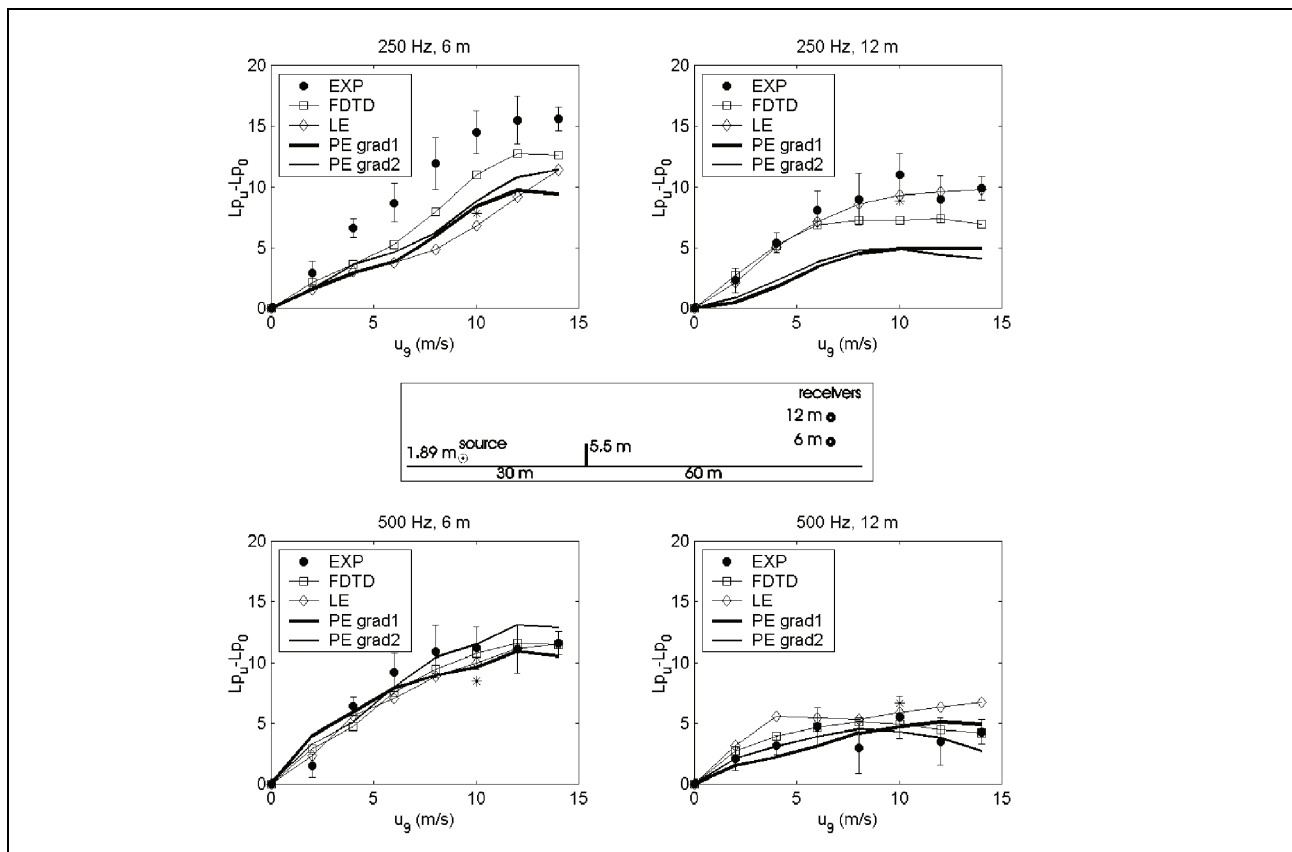


Figure 1. Comparison between the FDTD model, LE model by Blumrich and Heimann and the experimental results by Salomons. In abscis, the (incident) wind speed at a height of 9 m is shown, in ordinate the sound pressure level for the frequency band under consideration, for a certain wind speed, minus the SPL in absence of wind. The PE calculations by Salomons are indicated with PE grad1 and PE grad2, indicating the use of different sound speed gradients [3]. Measurements at a height of 6 m and 12 m are shown, for the octave bands at 250 Hz and 500 Hz. The * in the figures are the simulation results for FDTD, based on the same wind speed profiles as used during the LE calculations.

culations. All models simulate the experimental data well for the frequency band of 500 Hz.

For single noise barriers and the observation points considered, the approach of sound propagation in time-domain, taking into account time-invariant calculations of the flow, is capable to simulate the complex effect of wind on noise barrier performance. The screen-induced refraction of sound is well described by the proposed model.

5.2. Effect of windscreens on noise barrier performance

5.2.1. Experimental test set-up

In a wind tunnel experiment at scale [6], configurations of single noise barriers and noise barriers on either side of a line source were tested in combination with windscreens. The aim of this experiment was providing experimental data to check numerical schemes, and to investigate to what extent noise barrier performance for a typical traffic noise situation could be improved in wind. An overview of the tested configurations is given in Figure 2.

The wind direction was orthogonal to the noise barrier, and downwind sound propagation was studied. Two wind speeds, measured above the simulated atmospheric bound-

ary layer, were used. These were 6.4 m/s (further indicated in this paper as wind1) and 11 m/s (wind2). The height of the top of the boundary layer was approximately 60 cm [6]. At full scale, the frequency interval under investigation ranged from 500 Hz to 1 kHz, an important part of a typical traffic noise spectrum. A line source at ground level was constructed in the wind tunnel. Microphone positions were at distances ranging from 3H till 10H (where H indicates the noise barrier height, which was 0.18 m at scale) from the downwind noise barrier. Measurements were made at a height of 0.47H.

To simulate the wind reduction capacity of the canopy of trees, synthetic windscreens were used [6]. The porosity of the used windbreaks was about 32%. Such porosity results in a good global reduction of wind speed in a larger area downwind from the windscreen. Although the porosity of (a single row of) trees for most species ranges from 50% to 70%, lower porosity can be achieved with a single row of selected (dense) species (e.g. hedges or some spruce species), or by simply planting an extra row of trees close behind the other one [23].

The windscreens are acoustical neutral. The wind tunnel floor consisted of roughened plywood panels over the total length of the test section. The noise barriers were acousti-

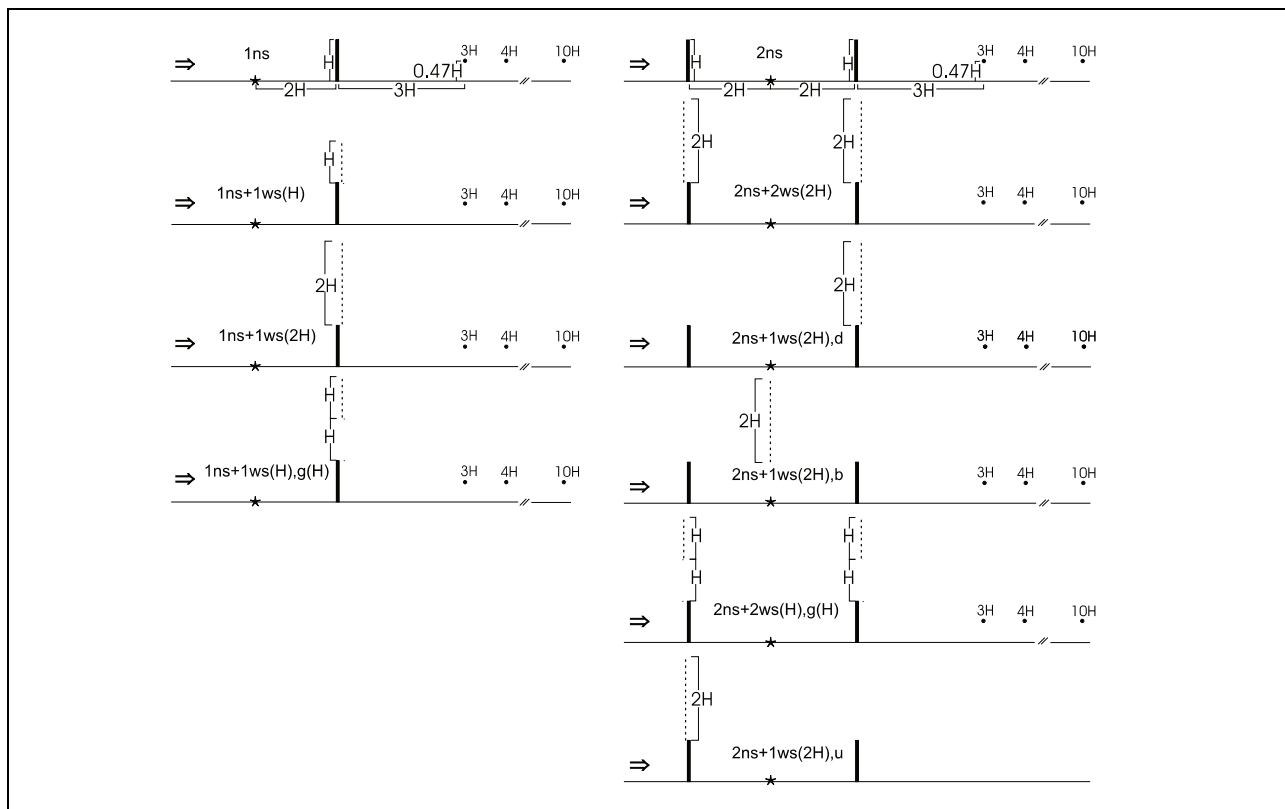


Figure 2. Overview of the tested configurations and their dimensions, relative to the noise barrier height. The configurations have the following codes: 1ns = 1 noise screen; 1ns+1ws(H) = 1 noise screen and 1 windscreen (height of windscreen = barrier height); 1ns+1ws(2H) = 1 noise screen and 1 windscreen (height of windscreen = 2 times the barrier height); 1ns+1ws(H),g(H) = 1 noise screen and 1 windscreen with a gap of length H in the windscreen; 2ns = 2 noise screens; 2ns+2ws(2H) = 2 noise screens and 2 windcreens; 2ns+1ws(2H),d = 2 noise screens and 1 windscreen, placed behind the downwind noise barrier; 2ns+1ws(2H),b = 2 noise screens and 1 windscreen, placed between the noise barriers; 2ns+2ws(H),g(H) = 2 noise screens and 2 windscreen, with a gap of length H in both windcreens; 2ns+1ws(2H),u = 2 noise screens and 1 windscreen, placed before the upwind noise barrier (only in simulations).

cally quite hard (see further). A detailed description of this experiment can be found in reference [6].

5.2.2. Extracting material parameters from measurements in absence of wind

Ground parameters were optimised for the ground model by Zwicker and Kosten (see section 4.1), based on measured sound levels with distance over flat ground without screens, in absence of wind. In Figure 3 (a), total sound pressure levels in the frequency interval 500-1000Hz at different locations in the wind tunnel are shown, relative to the first measure point. Following parameters (at scale) resulted in the best agreement with measurements, based on a trial-and-error procedure: $k_s = 1$, $\varphi = 0.5$, $R = 100 \text{ kPa s/m}^2$. Simulations with a perfectly reflecting noise barrier were compared to simulations where a slightly absorbing noise barrier was used. Applying a small absorption coefficient ($\alpha = 0.06$) at the surface of the barrier resulted in better agreement with experimental data.

The simulated insertion loss (IL) for both a single noise barrier and a noise barrier on either side of the line source is compared to experimental data in Figure 3b and 3c.

The differences between measurements and simulations, especially when noise barriers are present, are prob-

ably due to the experimental setup. However, the general trend observed in experimental results and simulations is similar.

5.2.3. Calculation of wind profiles including the effect of windcreens

Detailed wind profiles close to the barriers were calculated using the Computational Fluid Dynamics (CFD) software STAR-CD [18]. The numerical model assumes incompressible, quasi-static flow. The best correspondence between wind velocity calculations and experimental data is obtained using a steady state, $k-\varepsilon$ turbulence model [6]. A logarithmic wind speed profile is used as an inflow boundary condition:

$$v_z = \frac{u_*}{\kappa} \ln(z/z_0), \quad (29)$$

where z is the height above the surface, v_z is the velocity at height z , κ is the Von Karman constant ($= 0.4$ for air), u_* is the friction velocity and z_0 is the roughness length. Following parameters are used: $u_* = 0.77 \text{ m/s}$ and $z_0 = 1 \text{ mm}$ [6].

To model the effect of windcreens, the pressure drop as a function of flow velocity through the windcreens is inserted. Measurements in the velocity range of interest have

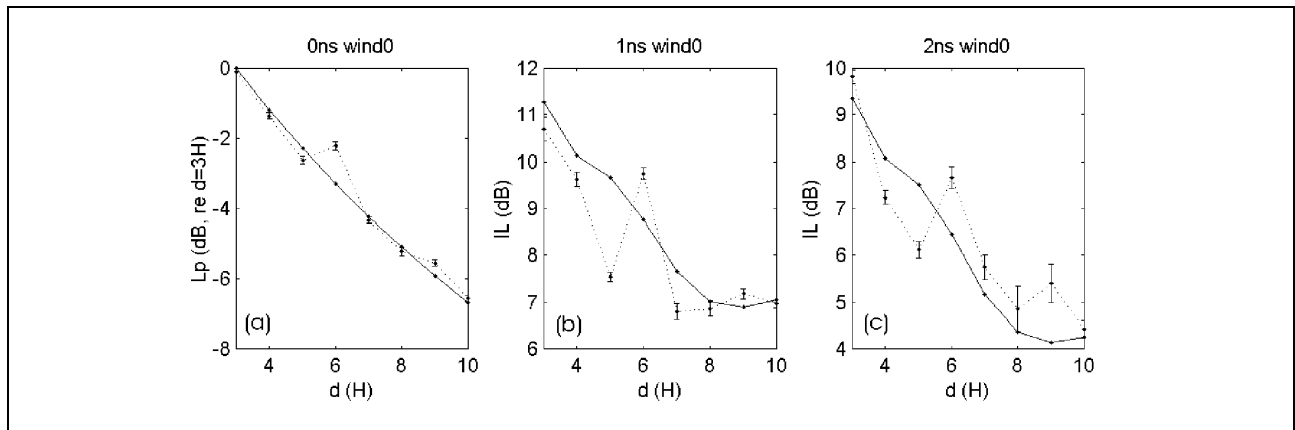


Figure 3. Results of fitting of both ground parameters and surface impedance of the noise barrier(s). In abscis, the distance relative to the location of the (downwind) noise barrier is shown, expressed in screen heights. In (a), total sound pressure levels for the frequency interval 500-1000 Hz, relative to the first measurement point, for flat ground without screens, are shown. In (b) and (c) the insertion loss is presented with increasing distance behind the downwind noise barrier, for respectively a single noise barrier and a double noise barrier. Parameter fitting was done in absence of wind. Experimental results are indicated by the dashed lines, FDTD simulations by the full lines. The errorbars on the experimental data are an indication of the standard deviation based on 20 independent measurements [6].

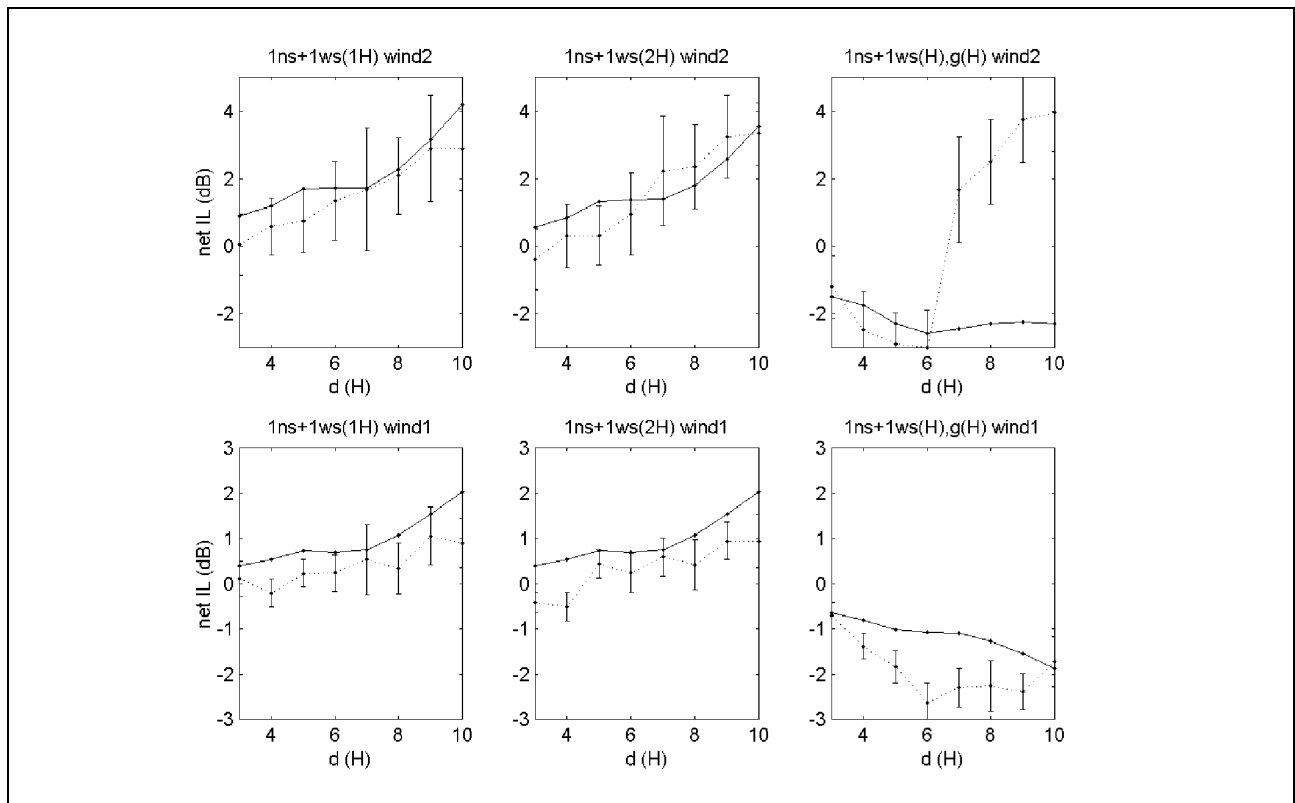


Figure 4. Comparison between FDTD simulations (full lines) and experimental results (dashed lines) for single noise barrier configurations. In the upper plots, the incident wind speed, measured above the boundary layer was 11 m/s (wind2), in the lower figures 6.4 m/s (wind1).

indicated that with high correlation the used windscreens can be described by the following quadratic equation:

$$\Delta p = av^2 + bv, \tag{30}$$

with $a = 5.040 \text{ Pa s}^2/\text{m}^2$ and $b = 0.092 \text{ Pa s/m}$ for a porosity of 32% [24].

5.2.4. Comparison of simulations with experimental data

The effect of the windscreens is quantified by their net insertion loss ($\text{net IL} = Lp_{u,x,ns,nows} - Lp_{u,x,ns,ws}$). This means, the sound pressure level in the frequency interval $f_1 - f_2$ for a noise barrier configuration (ns) with-

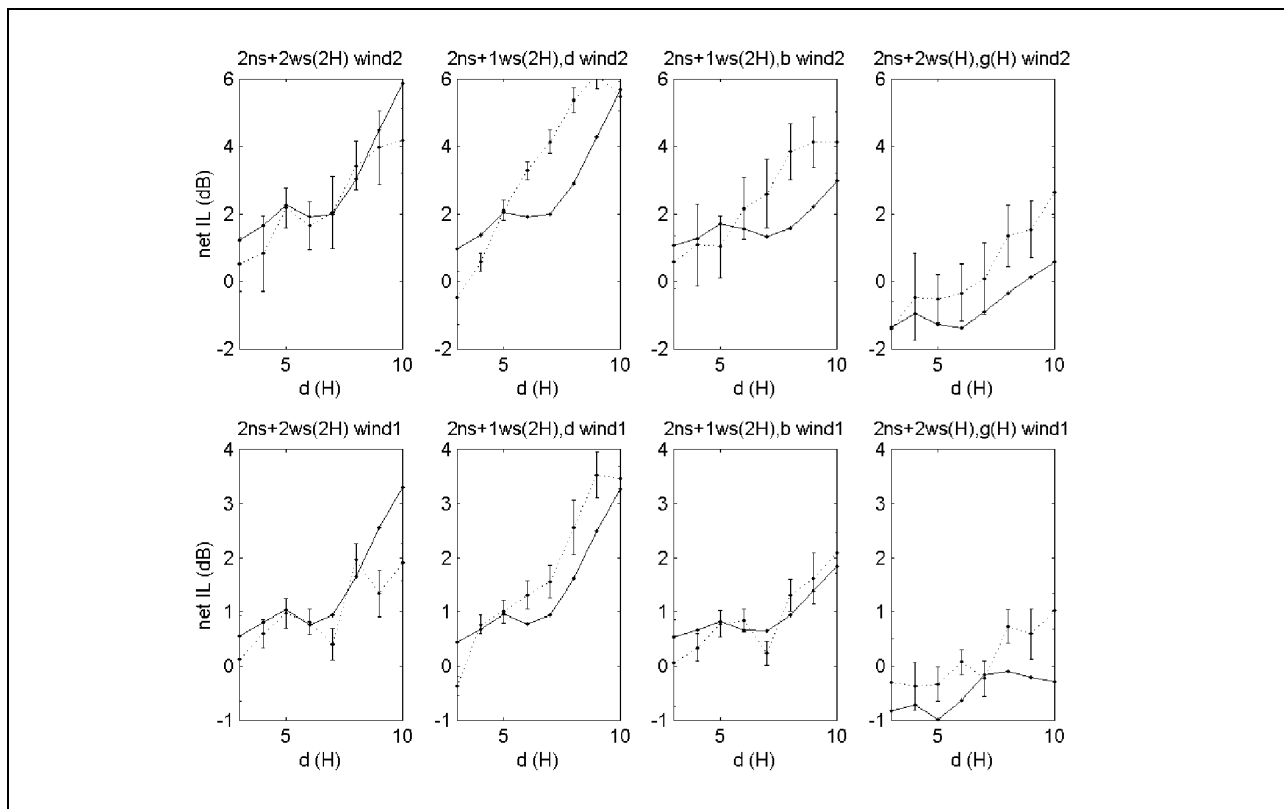


Figure 5. Comparison between FDTD simulations (full lines) and experimental results (dashed lines) for noise barriers on either side of the source. In the upper plots, the incident wind speed, measured above the boundary layer was 11 m/s, in the lower figures 6.4 m/s.

out windscreens ($Lp_{u,x,ns,now}$) is compared to the sound pressure level measured for the same noise barrier configuration (ns), at the same place x and for the same incident wind speed u , but now with the use of windscreens ($Lp_{u,x,ns,ws}$). In this way, the direct effect of placing a windscreen is obtained.

In Figures 4 and 5, a comparison between measured and numerically simulated net IL (for the frequency interval 500–1000 Hz) is made for respectively the single noise barrier configurations and the configurations where at either side of the source a noise barrier is present. Results are shown as a function of distance, for both the low wind speed (wind1) and the high wind speed (wind2) tested in the wind tunnel.

In general, the agreement between measurements and simulations is good. Besides the capability of the model to simulate screen-induced refraction of sound (as shown in section 5.1), the effect of wind reduction by windscreens or trees is well described.

Significant differences between measured and simulated data are observed for some double noise barrier configurations in combination with a large wind speed (wind2) (e.g. 2ns + 1ws(2H),d and 2ns + 1ws(2H),b). In contrast to e.g. situation 2ns+2ws(2H) where shielding by the windscreens is larger, a very complex and highly turbulent wind flow is observed, which makes these configurations more difficult to simulate accurately.

For the same reason, the configurations with a gap between windscreen and noise barrier (1ns+1ws(H), g(H)

and 2ns+2ws(H), g(H)) are also somewhat harder to simulate numerically, now also at wind1. However, trends and the negative effects observed with these configurations are predicted. The large discrepancy between measured and simulated net insertion loss for the single noise barrier case with a gap for wind2 (1ns+1ws(H), g(H)) could be due to experimental errors. This statement is confirmed by the observation that at low wind speeds these (relatively) large positive effects are not measured. Moreover, this is the only case where the trends observed at wind1 are not found at wind2 for the same configuration.

Turbulence is taken into account only during the CFD. For the acoustic calculations however, coherence loss due to turbulence and scattering on instantaneous fluctuations in atmosphere is not considered. Nevertheless, most configurations are adequately modelled. Since we are interested in the total effect of frequency intervals, it is expected that effects due to the variable nature of the flow are averaged out. Taking into account these phenomena might improve the correspondence between measurements and simulations even more.

6. Detailed analysis of using windscreens with noise barriers in wind by means of FDTD simulations

Windbreaks are defined as structures that reduce wind speed, not only at the structure itself, but also at a cer-

tain windward and leeward distance (e.g. rows of trees or synthetic windscreens). When simulating or measuring the effect of windbreaks on wind profiles, porosity is the major property [23]. In this view, the synthetic windscreens that are modelled throughout this paper can be used as a model for a row of trees with similar porosity.

In sections 6.1, 6.2 and 6.3, some parameters involved in the design of optimal configuration of windscreens are analysed. The results are presented for only one configuration, a single noise barrier with a large windscreen behind it (1ns+1ws(2H)) and for a source emitting a flat frequency spectrum between 250 and 500 Hz. In section 6.4, the global effect of the different windscreen configurations is investigated for a typical traffic noise spectrum.

Unless otherwise stated, following parameters are used during the simulations. The configurations of noise barriers and windscreens, as shown in Figure 2, are used. Two-dimensional sound propagation is studied: both the noise barrier(s) and line source are infinite long. The distance between the line source and the noise barrier(s) is in all cases 2H (with H is the height of the noise barrier), except in section 6.3, where the distance between source and noise barrier is investigated explicitly. The noise barriers are perfectly reflecting. The logarithmic wind speed profile described by equation (28) is used at the inflow. Wind is labelled by the speed at a height of 10 m above the ground surface, well within the atmospheric boundary layer. The ground in between the noise barriers is perfectly hard, while behind the noise barriers a very soft ground is used ($R = 5 \text{ kPa s/m}^2$ at full scale). For the single noise barrier configurations, the ground surface in the whole region upwind from the noise barrier is perfectly reflecting. In this way, the effect of both street surface coverage (hard) and natural soils (soft) are taken into account and the range of possible ground effects is maximised.

The “region of interest” is defined as the rectangular area behind the (downwind) noise barrier, up to a distance of 20H and up to a height of 1H. The distribution of the relevant quantities (e.g. net IL) are computed in this zone on a two-dimensional grid with observation points that are apart from each other at distances that equal $1/10^{\text{th}}$ of the highest wavelength under consideration. In this way, global effects of the parameters analysed and the different windscreen-configurations will be presented in a condensed and sufficiently accurate way.

6.1. Effect of porosity of windscreens

It is important to analyse the sensitivity of the positive effect of windscreens or the canopy of a row of trees on porosity to quantify the effect of e.g. deciduous trees throughout the year. The pressure drop of various windscreens as a function of flow velocity, for porosities ranging from 6% till 90%, was measured in detail [24]. These materials could be described accurately in the velocity range of interest by equation (30). The values for the parameters *a* and *b* as used during the flow calculations in this paper are presented in Table I.

Table I. Values for parameters *a* and *b*, to be used in equation (30) [24].

porosity [-]	<i>a</i> (Pa s ² /m ²)	<i>b</i> (Pa s/m)
0.16	54.313	-24.214
0.32	5.040	0.092
0.47	1.538	-0.533
0.59	0.842	0.553
0.76	0.491	-0.248

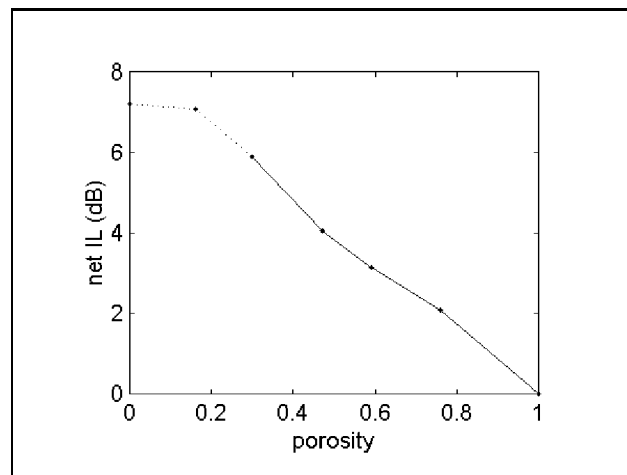


Figure 6. Net IL with decreasing porosity for frequency interval 250–500 Hz at a height of 0.5H, and at a distance of 7H downwind from the noise barrier. Configuration 1ns+1ws(2H) is simulated. The wind speed was 11 m/s. For porosities lower than 0.3 a pointed line is used: these simulations do not represent a physical situation since acoustic shielding is not accounted for.

During the experiment, a porosity of 32% has shown to be acoustical neutral. Lower porosities may result in acoustical shielding and scattering. For porosities down to about 30%, the screens are proven to be acoustical neutral. Simulations, neglecting these acoustic effects for very low porosity-screens (<30%), indicated that with decreasing porosity the (theoretical) net IL will increase and eventually reaches an asymptotic value (see Figure 6).

The distribution of observations in the region of interest (as defined in the beginning of this section) over 1-dB net IL-intervals for different porosities, is shown in Figure 7. For each curve, the sum of the fractions over all net IL-intervals equals one. The magnitude of the total wind effect (WE, this is the difference in sound pressure level of a noise barrier in absence of windscreens, with and without wind) is also presented. With increasing porosity, the maximum in the distribution is more pronounced, and the region where placing trees causes negative effects is larger. The high net IL classes become more populated with decreasing porosity. In general, a low porosity of the canopy of trees results in a better performance in wind. However, when looking at specific places in the region of interest, a higher porosity may sometimes result in a better performance due to a combination of the ground effect and the influence of the flow field.

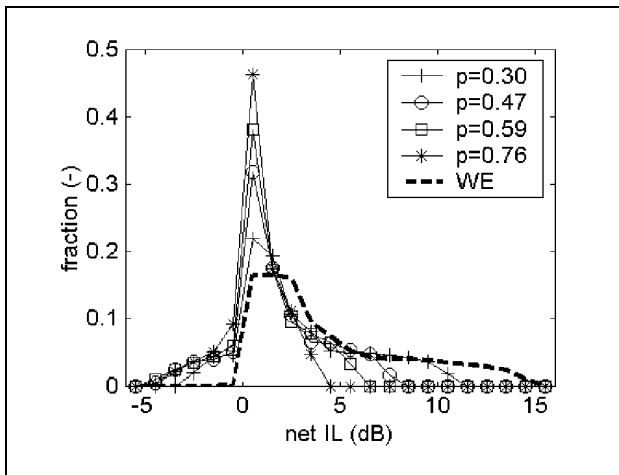


Figure 7. Distribution of net IL and WE for the frequency interval 250–500 Hz, in the region of interest for various porosities, ranging from 0.30 to 0.76. Configuration 1ns+1ws(2H) is simulated. The wind speed was 11 m/s.

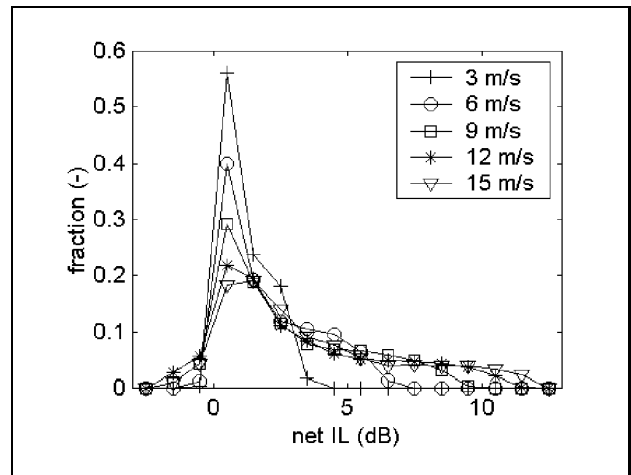


Figure 9. Distribution of net IL in the region of interest, for the frequency interval 250–500 Hz, for various incident wind speeds. Configuration 1ns+1ws(2H) is simulated (with a porosity of 30%).

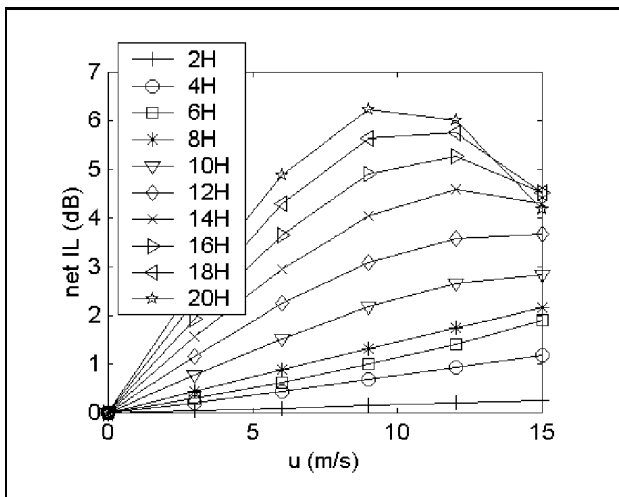


Figure 8. Net IL with increasing distance downwind from the noise barrier at a fixed height ($= 0.5H$). Results for the frequency interval 250–500 Hz are shown, for various incident wind speeds. Configuration 1ns+1ws(2H) is simulated (with a porosity of 30%).

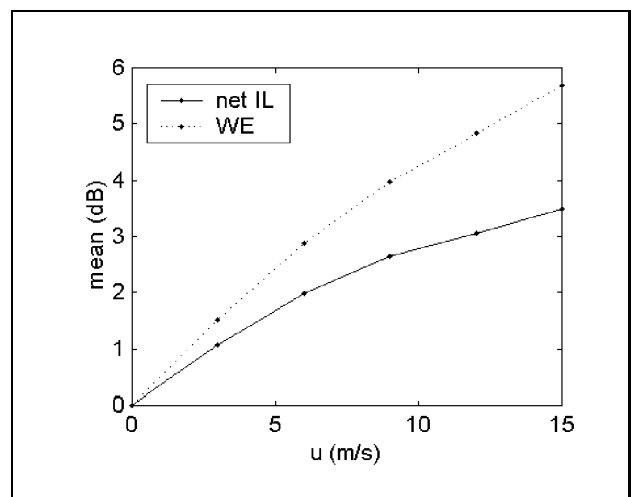


Figure 10. Average values of WE and net IL, for the frequency interval 250–500 Hz, in the region of interest, with increasing incident wind speed. The same data as in Figure 9 is used.

6.2. Effect of wind speed

In a field experiment along a highway [7], simultaneous measurements were done at a location with and without a row of trees behind a noise barrier. In this way, the effect of the trees could be compared directly. An almost linear relationship between wind speed and net IL was found for wind speeds ranging from 1 m/s up to 10 m/s. The microphones were placed at a distance of 9 times the barrier height behind it and at a height of 0.8H during this experiment [7].

To analyse the effect of wind speed on net IL numerically, calculations for wind speeds ranging from 3 m/s till 15 m/s are performed. A windscreens with a porosity of 0.30 is used. Net IL with distance for receiver positions at a height of 0.5H is shown in Figure 8. For distances closer

than 10H, the linear relationship between wind speed and net IL observed during the field experiment is recovered. At larger distances, this trend is not preserved and a maximum is observed: high wind speeds do not result anymore in the highest values for net IL. The overall effect of wind speed in the region of interest is illustrated with the histograms in Figure 9. More compact information is shown in Figure 10 by means of the numerical average over the region of interest of the WE and net IL with increasing wind velocity. The WE and net IL increase with increasing wind speed. For low wind speeds, net IL better approximates the WE than at higher wind speeds. Figure 9 reveals that with increasing wind speed, the high net IL classes get larger fractions in the distribution. For low wind speeds, the fractions present in the negative net IL classes are somewhat smaller.

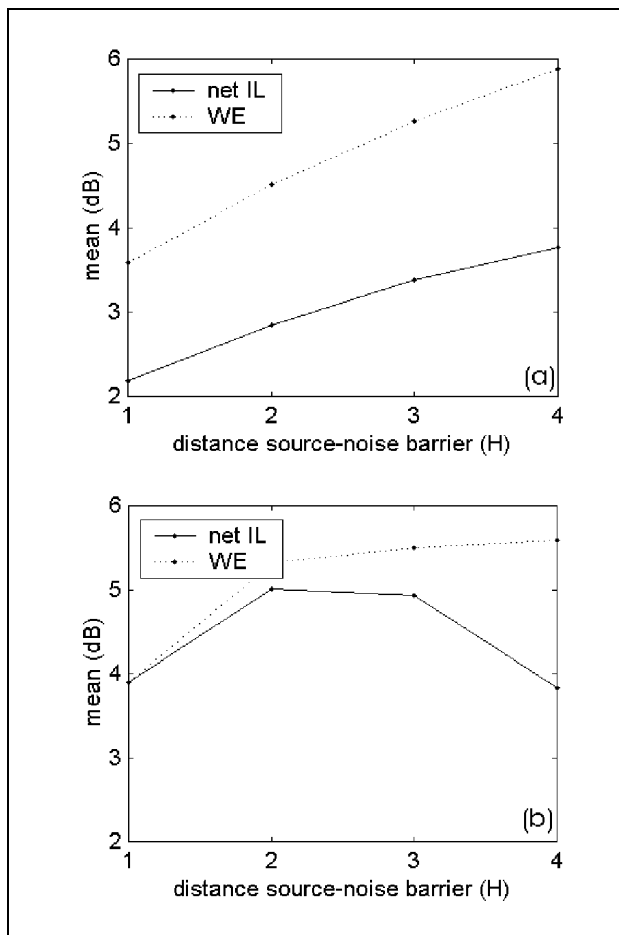


Figure 11. Average values of net IL (for configurations 1ns+1ws(2H) (a) and 2ns+1ws(2H),d (b)) and WE (for a single noise barrier (a) and a noise barrier on either side of the source (b)) for the frequency interval 250–500 Hz, in the region of interest, with increasing distance between source and noise barrier. A wind speed of 11 m/s and a porosity of 0.3 are used.

6.3. Effect of distance between source and noise barrier(s)

It is investigated how the magnitude of the WE and net IL behave with increasing distance between the noise source and the noise barrier. Simulations are performed for a windscreen with a porosity of 30% and for an incident wind speed of 11 m/s (at a height of 10 m). In Figure 11, the average WE and net IL in the region of interest are shown with increasing distance between the line source and the barrier(s), for both a single noise barrier configuration (a) and a noise barrier on either side of the source (b). A large windscreen (2H) is placed behind the (downwind) noise barrier in both cases. In general, the positive effect of the windscreen is larger in the double noise barrier situation.

When the source is moved away from the barrier, the effect of wind increases. For the single noise barrier configuration, net IL follows this trend, and the ratio between WE and net IL stays almost the same for the distances under consideration. When a noise barrier is present on both sides of the source, WE initially grows faster with

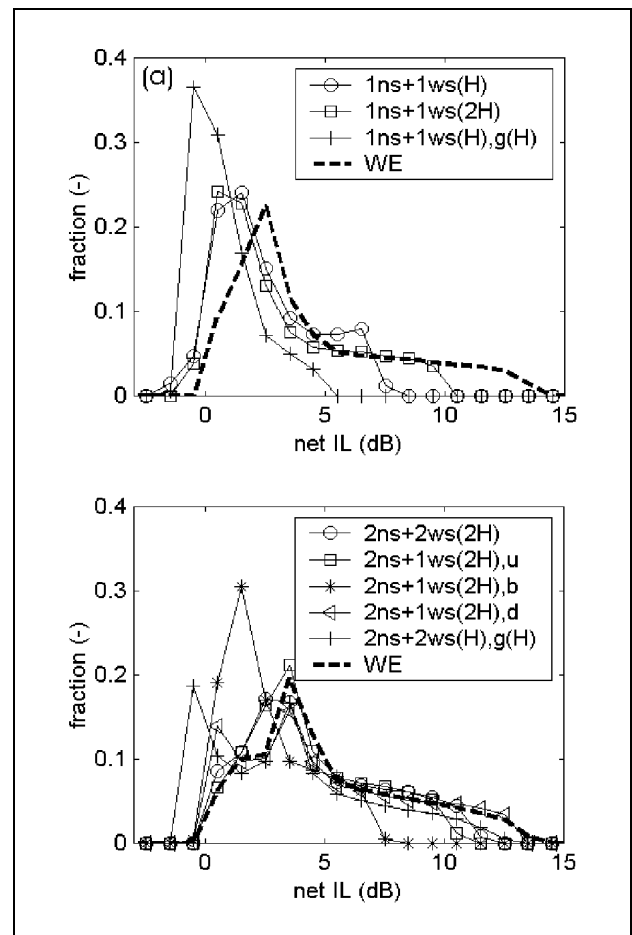


Figure 12. Distribution of the net IL regarding total sound pressure levels resulting from typical traffic noise, for different configurations of windscreens, applied to single noise barriers (a) and noise barriers on either side of the source (b), in the region of interest (as defined in the beginning of section 6). A wind speed of 11 m/s and a porosity of 0.3 are used. The magnitude of the wind effect (WE) is also shown.

distance. The efficiency of the windscreen for small distances between source and barrier is higher but decreases for larger distances. At very limited distances between the source and noise barrier (e.g. 1H), wind effects are completely neutralised, in contrast to the single noise barrier configuration. It is expected that for large distances between the source and the noise barriers, effects from the upwind noise barrier will become negligible, and as a result, the same behaviour will be observed as for a single noise barrier.

6.4. Global effect of the different windscreen configurations for traffic noise

Finally we analyse the effect of windscreens for the configurations given in Figure 2 in the region of interest, as defined in the beginning of the section, for a typical traffic noise spectrum. The wind speed at a height of 10 m above the surface was 11 m/s. In Figure 12a and 12b, the distribution of the observations in the region of interest over net IL for the different configurations of windscreens (with a

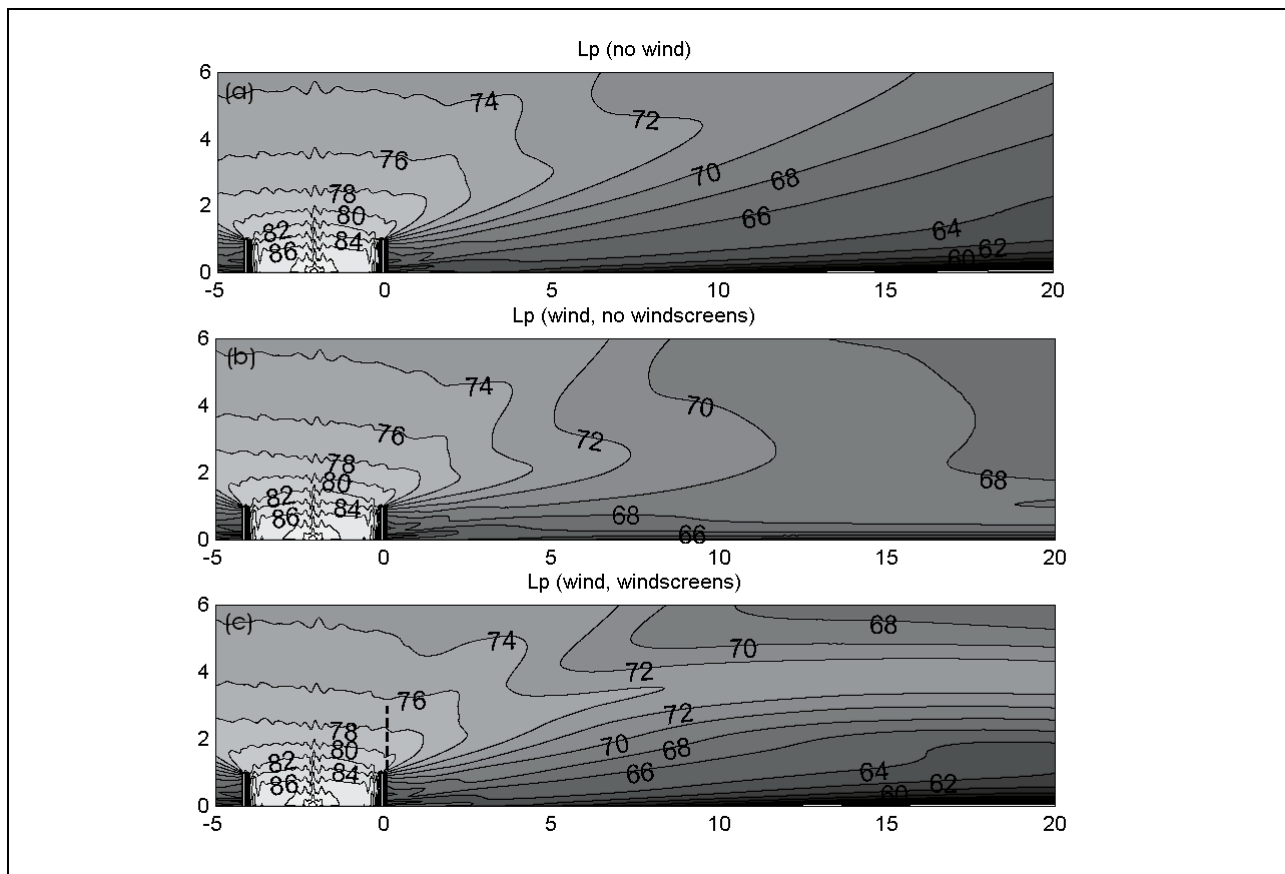


Figure 13. Numerically simulated sound pressure levels in absence of wind (a), in presence of wind (without windscreens) (b) and in presence of both wind and a large windscreen (2H, porosity of 30%) behind the downwind noise barrier (c), for a typical traffic noise spectrum. Distances and heights are expressed in noise barrier heights. The values in the field plots are in dB.

porosity of 0.3), for respectively single noise barriers and noise barriers on either side of the line source, is shown. The magnitude of the wind effect (WE) is also presented in Figure 12. Placing a large windscreen (2H) behind a single noise barrier instead of a smaller one (1H) does not result in a significant improvement. Only the small fraction in the high net IL classes is somewhat larger. The maximum of both distributions is observed between 1 and 2 dB.

The configuration with noise barriers on either side of the road and windscreens linked up to the barriers (2ns+1ws(2H),u; 2ns+1ws(2H),d and 2ns+2ws(2H)) do not behave very differently, except for the fractions observed in the very high net IL classes. A maximum in the distribution of net IL for these configurations is found between 3 and 4 dB. Using a windscreen in between the noise barriers (2ns+1ws(2H),b) results in a more limited improvement: a sharp maximum is observed in the distribution between 1 and 2 dB. In contrast to the single noise barrier configurations, it is possible to almost completely cancel the effect of wind (in the region of interest) when looking at total sound pressure levels resulting from traffic noise for noise barriers on either side of the road. The distribution of the magnitude of the wind effect (WE) and the distribution of some windscreen-configurations are indeed very close to each other.

In the wind tunnel experiment [6], it was observed that the configurations with a gap between noise barrier and windscreen result in negative net IL at the distances investigated (<10H). It is shown in Figure 12 that for the single noise barrier configuration, the maximum in the distribution of net IL values is negative. For the double noise barrier configuration with gaps in the windscreens, a local maximum is observed at negative values for net IL. In general, large gaps in the windscreens should be avoided because negative net IL by using windscreens is observed, especially close to the noise barrier(s).

In Figure 13 and 14, more detailed information is shown by means of field plots for the configurations consisting of two noise barriers, for a typical traffic noise spectrum and for a wind speed of 11 m/s. In Figure 13, sound pressure levels are shown in absence of wind (a), in presence of wind (without windscreens) (b) and in presence of both wind and a large windscreen behind the downwind noise barrier (2ns+1ws(2H),d) (c). In Figure 14 the insertion loss in absence of wind (a) is shown together with some quantities derived from Figure 11: namely the magnitude of the WE (b) and the net IL or the improvement by placing a windscreen behind the downwind noise barrier (c). In both figures, an area up to a distance of 20H behind the downwind noise barrier and up to a height of 6H is shown. The effect of wind is significant: a decrease in bar-

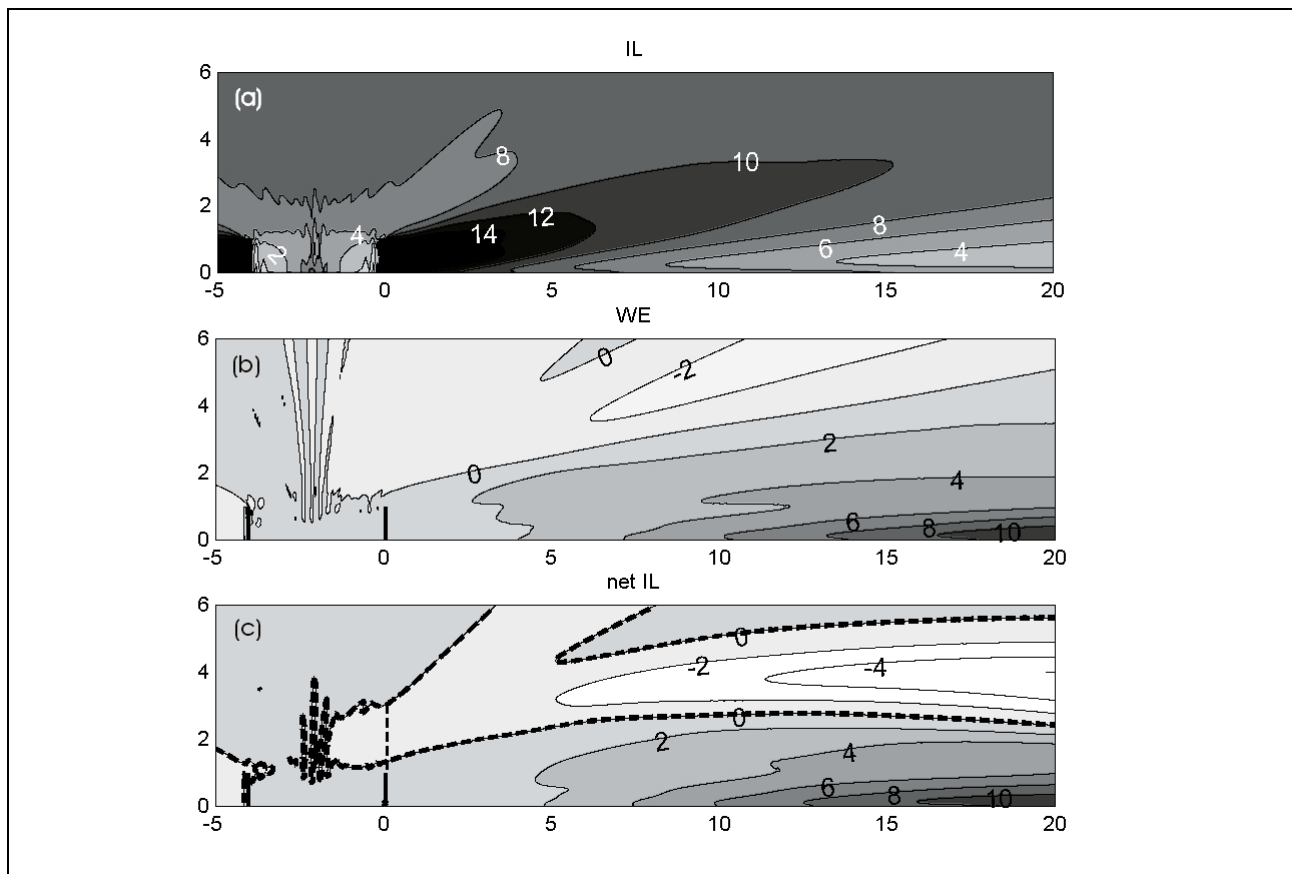


Figure 14. Numerically simulated IL in absence of wind (a), the magnitude of the wind effect (WE) (b) and the net IL, as a result of placing a windscreen (2H, porosity of 30%) behind the downwind noise barrier (c), for a typical traffic noise spectrum. Distances and heights are expressed in noise barrier heights. The values in the field plots are in dB.

rier efficiency of more than 10 dB is noticed at distances larger than 15H (see Figure 14b). The region in which improvement (net IL > 0dB) is observed by placing a row of trees behind the noise barrier is bordered by the dashed, tick black line in Figure 14c. The main zone of interest for noise reduction by barriers is covered. At most places, the net IL approximates the WE for this configuration of windcreens, indicating that wind effects are neutralised.

7. Conclusion

The time-domain numerical model based on separating flow and acoustics in the fluid dynamic equations, which is presented in this paper, was shown to be a valuable simulation technique to account for complex wind fields emerging around noise barriers. It was shown that the screen-induced refraction of sound by wind for a single noise barrier is accurately modelled by comparing insertion loss to results of scale experiments and other numerical models. Also, the effect of windcreens or rows of trees on noise barrier performance in wind, which was observed in experiments, seems adequately simulated. Perfectly absorbing boundaries are used to limit the simulation region at the upper and lateral ends. The Perfectly Matched Layer (PML) technique was adapted to account for moving me-

dia for this purpose. Applying such a boundary condition makes it possible to simulate typical traffic noise situations, where the source is in between the noise barriers and the impulse response is quite long due to multiple reflections.

A region of interest was defined, up to a distance of 20H behind the downwind noise barrier and up to a height of 1H. Simulations revealed that the porosity of the windcreens is an important parameter. In general, decreasing porosity results in a better performance. With increasing wind speed, the effect of the windcreens becomes in general larger. When the distance between source and noise barrier increases, wind effects become larger. The net IL increases proportionally with the wind effect for a single noise barrier configuration up to a distance of 4H between source and barrier. When noise barriers are present at both sides of the source, the decrease of noise barrier performance by wind can be completely neutralised by the windcreens for small distances between barrier and source. For larger distances between the source and noise barrier (>2H), the trend of the screen-induced refraction is not followed anymore.

Different locations of windcreens are investigated numerically for the configuration where at either side of the line source a noise barrier is present. The best overall performance in the region of interest is observed for wind-

screens linking up to the noise barriers. It is possible to almost completely cancel the effect of wind on noise barrier performance when looking at total sound pressure levels resulting from traffic noise in this region.

Gaps between the noise barrier and windscreen result in negative effects at short distances from the (downwind) noise barrier ($<10H$), and should therefore be avoided.

Acknowledgement

The authors would like to thank E. M. Salomons, R. Blumrich and D. Heimann for providing experimental data and simulation results on the wind tunnel experiment described in reference [3] and for fruitful discussion.

References

- [1] R. DeJong, E. Stusnick: Scale model studies of the effect of wind on acoustic barrier performance. *Noise control engineering* **6** (1976) 101–109.
- [2] K. B. Rasmussen, M. G. Arranz: The insertion loss of screens under the influence of wind. *J. Acoust. Soc. Am.* **104** (1998) 2692–2698.
- [3] E. M. Salomons: Reduction of the performance of a noise screen due to screen-induced wind-speed gradients. numerical computations and wind tunnel experiments. *J. Acoust. Soc. Am.* **105** (1999) 2287–2293.
- [4] N. Barriere, Y. Gabillet: Sound propagation over a barrier with realistic wind gradients. Comparison of wind tunnel experiments with GFPE computations. *Acustica – Acta acustica* **85** (1999) 325–334.
- [5] D. Heimann, R. Blumrich: Modeling the wind effect on the acoustical performance of various screen geometries. 9th International Congress on Sound and Vibration, Orlando, 2001.
- [6] T. Van Renterghem, D. Botteldooren, W. Cornelis, D. Gabriels: Reducing screen-induced refraction of noise barriers in wind by vegetative screens. *Acustica – Acta acustica* **88** (2002) 231–238.
- [7] T. Van Renterghem, D. Botteldooren: Effect of a row of trees behind noise barriers in wind. *Acustica – Acta acustica* **88** (2002) 869–878.
- [8] K. Attenborough, S. Taherzadeh, H. E. Bass, X. Di, R. Raspet, G. R. Becker, A. Guedesen, A. Chrestman, G. A. Daigle, A. L'Esperance, Y. Gabillet, K. E. Gilbert, Y. L. Li, M. J. White, P. Naz, J. M. Noble, H. A. J. M. van Hoof: Benchmarks cases for outdoor sound propagation models. *J. Acoust. Soc. Am.* **97** (1995) 173–191.
- [9] E. M. Salomons: *Computational atmospheric acoustics*. Kluwer, Dordrecht, 2001.
- [10] E. Premat, Y. Gabillet: A new boundary-element method for predicting outdoor sound propagation and application to the case of a sound barrier in the presence of downward refraction. *J. Acoust. Soc. Am.* **108** (2000) 2775–2783.
- [11] R. Raspet, G. Baird, W. Wu: Normal mode solution for low-frequency sound propagation in a downward refracting atmosphere above a complex impedance plane. *J. Acoust. Soc. Am.* **91** (1992) 1341–1352.
- [12] D. Botteldooren: Acoustical finite-difference time-domain simulations in a quasi-Cartesian grid. *J. Acoust. Soc. Am.* **95** (1994) 2313–2319.
- [13] D. Botteldooren: Time-domain simulation of the influence of close barriers on sound propagation to the environment. *J. Acoust. Soc. Am.* **101** (1997) 1278–1285.
- [14] R. Blumrich, D. Heimann: A linearized Eulerian sound propagation model for studies of complex meteorological effects. *J. Acoust. Soc. Am.* **112** (2002) 446–455.
- [15] C. Zwikker, C. W. Kosten: *Sound absorbing materials*. Elsevier, New York, 1949.
- [16] E. M. Salomons, R. Blumrich, D. Heimann: Eulerian time-domain model for sound propagation over a finite-impedance ground surface. Comparison with frequency-domain models. *Acustica – Acta acustica* **88** (2002) 483–492.
- [17] J. H. Ferziger, M. Peric: *Computational methods for fluid dynamics*. New York, Springer, 1997.
- [18] *Computational dynamics LTD: STAR-CD (Version 3.1A)*. London, 2000.
- [19] D. Botteldooren: Finite-difference time-domain simulation of low-frequency room acoustic problems. *J. Acoust. Soc. Am.* **98** (1995) 3302–3308.
- [20] M. A. Biot: Theory of propagation of elastic waves in a fluid-saturated porous solid. I. Low frequency range **28** (1956) 168–178.
- [21] J. P. Berenger: A perfectly matched layer for the absorption of electromagnetic waves. *J. Comp. Physics* **114** (1994) 185–200.
- [22] J. P. Berenger: Perfectly matched layer for the FDTD solution of wavestructure interaction problems. *IEEE Antennas Propagation Symposium* **44** (1996) 110–117.
- [23] L. J. Hagen, E. L. Skidmore: Windbreak drag as influenced by porosity. *Transactions of the American Society of Agricultural Engineers* **14** (1971) 464–465.
- [24] W. Dierickx: Flow reduction of synthetic screens obtained with both a water and airflow apparatus. *J. Agric. Eng. Res.* **71** (1998) 67–73.